Microgravity Science and Technology (2022) 34: 71
https://doi.org/10.1007/s12217-022-09996-7

ORIGINAL ARTICLE

Hypergravity Effect on Dynamic Capillary Flow in Inclined Conical Tubes with Undulated Inner Walls

Jie-Chao Lei[1,2] · Haochen Sun[1,2] · Shaobao Liu[1,2] · Shangsheng Feng[3,4] · Tian Jian Lu[1,2]

Received: 23 March 2022 / Accepted: 20 July 2022 / Published online: 2 August 2022

Abstract

Capillaries in human brain and plants are often neither straight nor smooth, but exhibit conical tubes with numerous wall undulations. Under hypergravity, the dynamics of blood/water flow in such roughened conical capillaries remains elusive, which may affect the performance and health of pilots/astronauts and the growth of plants. This study aims to establish a theoretical model to characterize dynamic capillary rise in inclined conical tubes having idealized cosine-type undulated inner walls, with hypergravity effect duly accounted for. For validation, full numerical simulations are performed, and good agreement is achieved between theoretical and numerical results. Dynamic capillary rise in undulated conical tubes is shown to be strongly dependent upon three key morphology parameters: undulation amplitude and axial wave number of cosine-type wall, and opening angle (either positive or negative) of conical tube. The steady height of capillary rise decreases with increasing opening angle (positive) and/or increasing undulation amplitude for moderate wave numbers, but increases when the opening angle is negative or the wave number is small. When the wave number becomes sufficiently large, the steady height increases with increasing amplitude and decreases with increasing wave number. In the presence of hypergravity effect, the dynamics of capillary rise in undulated conical tubes for several commonly used liquid types is explored to provide theoretical guidance for practical applications in the fields of aeronautical engineering, space exploitation, and the like.

Keywords Capillary flow · Conical tube · Undulation · Dynamics · Hypergravity

Introduction

Hypergravity is often encountered in aerospace engineering, e.g., during aerobatic maneuvers of aircrafts, launching of space vehicles, and re-orbiting maneuvers of spacecrafts. Correspondingly, the influence of hydrostatic forces on fluid flow in narrow channels becomes important, e.g., driving force of liquid flow in microfluidic devices (Culbertson et al. 2005; Kundan et al. 2015), cooling capacity of electronic devices (Iceri et al. 2020), delivery of lubricating oil in aerocrafts (Oikonomidou et al. 2019), and the like. Also, under such conditions, hypergravity can affect blood transport and cause severe health problems for pilots and astronauts (Bureau et al. 2017), such as headache, loss of vision, loss of consciousness, and even death (van Geel et al. 2010). Further, while numerous studies have shown that hypergravity significantly affects the growth of plants (Downey et al. 2013; Vidyasagar et al. 2014), the dynamics of nutrient uptake by plants in hypergravity environment remains poorly understood. It is therefore of necessity and practical significance to explore systematically the dynamics of capillary flow under hypergravity.

Assuming that a porous medium could be simplified as "a bundle of capillary tubes", Lucas (1918) developed the model of capillary imbibition to reveal the dynamics underlying capillary flow in porous media. Subsequently, Washburn

✉ Tian Jian Lu
tjlu@nuaa.edu.cn

1 State Key Laboratory of Mechanics and Control of Mechanical Structures, Nanjing University of Aeronautics and Astronautics, Nanjing 210016, People's Republic of China

2 MIIT Key Laboratory of Multifunctional Lightweight Materials and Structures, Nanjing University of Aeronautics and Astronautics, Nanjing 21006, People's Republic of China

3 Bioinspired Engineering and Biomechanics Center (BEBC), Xi'an Jiaotong University, Xi'an 710049, People's Republic of China

4 School of Life Science and Technology, The Key Laboratory of Biomedical Information Engineering of Ministry of Education, Xi'an Jiaotong University, Xi'an 710049, People's Republic of China

(1921) improved the model and presented an equation to quantify capillary height in a circular smooth tube. At present, the Lucas-Washburn (LW) equation is one of the most commonly adopted models to study capillary rise in smooth tubes/channels. However, while inertia was neglected by the LW equation, it has now been well established that inertia has important influence on capillary height and velocity during the initial stage of capillary rise. For instance, Bosanquet (1923) and Quéré (1997) addressed this issue in detail and presented relevant analytical solutions. More recently, to further improve the understanding of spontaneous capillary phenomenon, dimensionless analysis of dynamic capillary rise in a circular tube and a rectangular channel, both having smooth walls, were separately carried out by applying the Buckingham π theorem (Fries and Dreyer 2009; Ouali et al. 2013). Nonetheless, it must be pointed out that, while existing studies largely assumed that the flow channels have smooth walls, in realistic applications, they often exhibit undulated (roughened) inner walls, or have capillary ratchets. Non-smooth surface structures significantly affect the contact angle, thus altering the capillary force and the dynamics of capillary flow (Heshmati and Piri 2014). For example, recently, it was found that the capillary ratchets of *Araucaria* leaf have the ability to control the spreading direction and capillary height for different fluids (Feng et al. 2021). Consequently, in addition to hypergravity, it is also of importance to quantify the effect of wall morphology (surface roughness) on dynamic capillary flow.

With Wenzel's law (Wenzel 1936) and the slope of wall profile (Shuttleworth and Bailey 1948) commonly employed to describe the relationship between static contact angle and surface roughness/undulation (Bico et al. 2002; Hay et al. 2008; Malijevský 2014; Patel et al. 2019; Sudeepthi et al. 2020), capillary flow in an undulated (roughened) channel/tube has been investigated theoretically, numerically and experimentally: for instance, vertical capillary flow in tubes with nonuniform cross sections (Liou et al. 2009), horizontal capillary flow in conical tubes with smooth walls (Reyssat et al. 2008), capillary flow in vertical parabolic channels (Figliuzzi and Buie 2013), horizontal capillary flow in tubes with sinusoidal walls (Wang et al. 2013), vertical capillary rise in nano-channels having inherent surface roughness (Shen et al. 2017), and vertical capillary flow in a channel between two plates covered with cylindrical micropillar arrays (Kim et al. 2020). Recently, the present authors (Lei et al. 2021) presented a dimensionless analysis of dynamic capillary flow in circular tubes with cosinoidal wall undulations; it was found that, relative to smooth tubes, properly designed undulations serve to increase the capillary rising height. However, when the amplitude of undulation (roughness) becomes large, the Hagen-Poiseuille assumption adopted by previous theoretical model places a limitation on its applicability.

As aforementioned, during aerobatic maneuvers of aircrafts and launching of space vehicles, the pilots and astronauts often encounter hypergravity (van Geel et al. 2010). Further, as the vasculature of human brain is mainly composed of intricate capillary networks lined by capillary pericytes (Figs. 1a-d) (Hartmann et al. 2021; Cassot et al. 2006), capillary force is one of the important driving forces to promote blood flow and then task with delivery of oxygen and nutrients to billions of brain cells (Hartmann et al. 2021). Moreover, blood capillaries are neither straight nor smooth, but often exhibit conical tubes with numerous undulations on their inner walls (Figs. 1e and f) (Ando et al. 2018; Cassot et al. 2006). Up to now, the dynamics of blood flow in capillaries under hypergravity remains elusive, which may affect the performance and health of pilots and astronauts. In addition, the xylem network of plants often exhibits conical tubes with non-smooth walls, such as leaf veins (Fig. 2). Therefore, when studying the effect of hypergravity on growth of plants, the dynamics of capillary flow in undulated conical tubes must be accounted for (Kim et al. 2014; Guo et al. 2019). For both human being and plants, it is thus necessary to explore how hypergravity affects capillary flow in conical tubes with roughened inner walls.

The first goal of this study is to establish a theoretical model to quantify the effect of hypergravity upon capillary flow in conical tubes with idealized cosinoidal wall undulations; to expand the values of key morphological parameters (i.e., undulation amplitude and axial wave number of cosine-type wall, and opening angle of conical tube) beyond the range predicted by the model, numerical simulations are also performed. The second objective is to analyze capillary limitations of different liquid types and the corresponding time, so as to provide theoretical guidance for practical applications in, say, aeronautical engineering and space exploitation. For simplicity, the undulated wall of the conical tube is treated as rigid.

Model of Capillary Rise

According to the theorem of momentum, the dynamics of capillary flow in a smooth tube/channel can be described by (Bosanquet 1923; Shen et al. 2017):

$$F = \frac{d\left(m\dot{h}\right)}{dt} = F_{cap} - F_{vis} - F_g, \tag{1}$$

where m is the mass in a control volume of concern, and F_{cap}, F_{vis}, and F_g are the capillary, viscous, and gravitational forces, respectively. The viscous force and gravity counter the rise of fluid and do negative work, thus having the "−" signs in the front.

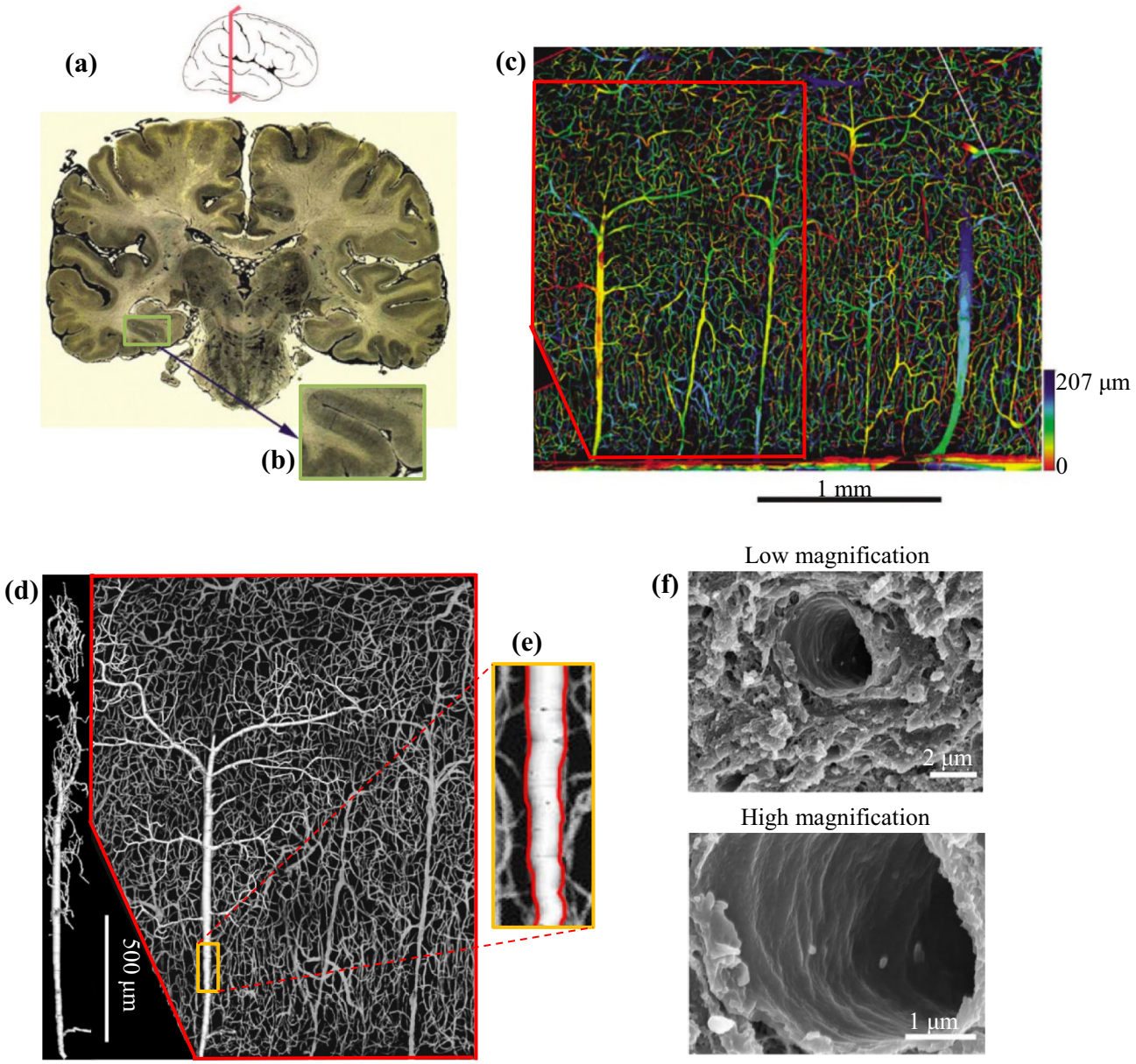

Fig. 1 Length scales for microvascular networks in human brain: **a** Brain scale (~63 $cm^2 \times 300$ μm): 300 μm-thick cortical section, where blood vessels have been injected with India ink for contrast enhancement (Cassot et al. 2006; Peyrounette et al. 2018), **b** collateral sulcus in the temporal lobe (Cassot et al. 2006), **c** depth coded projection of the zone reconstructed by confocal microscopy with the outlines (Cassot et al. 2006), **d** large vein extracted from network (left: side view, right: top view) (Cassot et al. 2006), **e** outlines of local blood vessel (red curves) (Cassot et al. 2006), and **f** cross section of blood capillary (upper: low magnification, lower: high magnification) (Ando et al. 2018)

Figure 3 illustrates schematically the phenomenon of dynamic capillary rise in a conical tube with idealized cosinoidal undulations (roughness) on its inner wall, inserted into a bulk incompressible viscous Newtonian fluid. The tube is oriented at an arbitrary angle ϕ relative to the horizontal surface of the fluid. Note that, the effect of hypergravity (large acceleration) directions on blood flow of pilots/astronauts, water transport in plants, and liquids transport in aerospace engineering is typically anisotropic (Vidyasagar et al. 2014; Akparibo et al. 2021). For example, for pilots and astronauts in service, the acceleration acting along cephalad-to-foot direction $+GZ$ (G: value of hypergravity/acceleration, "+": positive Z-direction) has more serious impact on blood flow than other directions, i.e., thoracic-to-dorsal direction $+GX$ and lateral direction $+GY$ (Akparibo et al. 2021). Therefore, in the present study, particular focus is placed upon hypergravity in the $+GZ$ direction, and its influence on dynamic capillary rise in an inclined conical

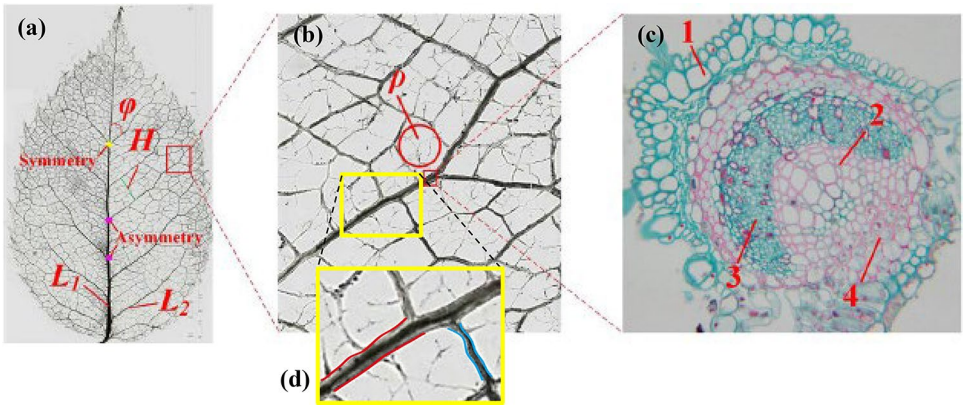

Fig. 2 Leaf vein structure of Zelkova: **a** image of leaf, **b** secondary vein, **c** transverse microstructures of secondary vein: 1-parenchyma cell; 2-vessel (~37 μm); 3-sieve tube (~55 μm); 4-collenchymatous cell, and **d** outlines of local veins (red curve: secondary vein; blue curve: tertiary vein (vessel: ~11 μm, sieve tube: ~18 μm)) (Guo et al. 2019)

tube with roughened inner walls is quantified by varying the azimuthal angle ϕ (Fig. 3).

The mathematical model characterizing the idealized conical tube of Fig. 3 is given by:

$$R(z) = R_0 + \beta z - e\cos\left(\frac{2\pi}{b}z\right) = R_0\left[1 + \beta\frac{z}{R_0} - \varepsilon\cos\left(\alpha\frac{z}{R_0}\right)\right], \tag{2}$$

where R_0 is the mean radius of conical tube, e and b are the amplitude and wavelength of cosinoidal undulation, ε is the ratio of e to R_0, $\alpha = 2\pi R_0/b$ is the dimensionless wave number of undulation, and $\beta = \pm d/L$ is the cone opening angle. A positive β corresponds to the case of gradually expanding tube diameter (Fig. 3a), while a negative β implies the opposite (Fig. 3b). A small α indicates that the inner wall is slightly undulated and hence may be taken approximately as smooth.

Upon inserting the roughened conical tube into a fluid, the capillary force brings up the fluid instantaneously, the latter reaching a steady height over a relatively long period, as shown in Fig. 3. To study how key morphological parameters of the tube, such as opening angle and amplitude/wave number of undulations, may affect the dynamic capillary rise, the relationship between these parameters and instantaneous capillary height $h(t)$ needs to be determined from Eq. (1).

With reference to Fig. 3, within the control volume enclosed by the undulated wall, $z=0$ and $z=h$, the rate of change in momentum is given by:

$$F = \frac{d(m\dot{h})}{dt} = \frac{d\left(\pi\rho\int_0^h R^2(z)dz\dot{h}\right)}{dt}, \tag{3}$$

where ρ is the density of fluid.

Due to the presence of wall undulations (Fig. 3), the apparent contact angle φ is different from the static contact angle θ, thus altering the capillary force relative to the case of a smooth conical tube. In the present study, the slope of wall profile is used to connect the two contact angles, as (Figliuzzi and Buie 2013; Shuttleworth and Bailey 1948):

$$\varphi = \theta + \arctan\left(\frac{dR}{dz}(h)\right). \tag{4}$$

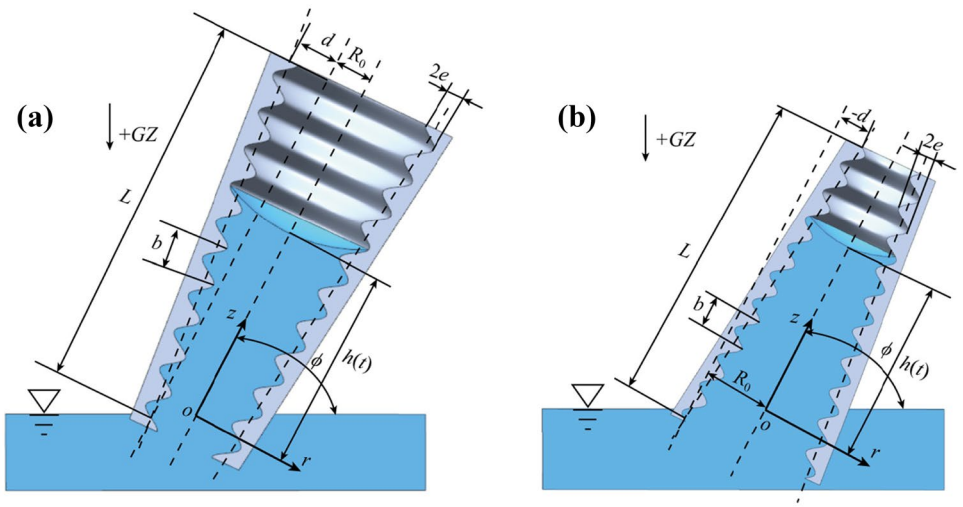

Fig. 3 Dynamic capillary rise in a conical tube with cosinoidally undulated inner wall: **a** positive opening angle and **b** negative opening angle. R_0 is mean radius of tube, e is undulation amplitude, b is undulation wavelength, $\beta = \pm d/L$ is cone opening angle, ϕ ($0 \le \phi \le \pi/2$) is inclination angle of tube, and $+GZ$ is Z-direction acceleration (G: value of hypergravity/acceleration), and $h(t)$ is height of meniscus at time t

It follows that the capillary force altered by wall undulations can be obtained by using the Young–Laplace equation, as:

$$F_{cap} = 2\gamma \frac{\cos(\varphi)}{R(h)} \pi R^2(h), \tag{5}$$

where γ is the surface tension of fluid.

The Hagen-Poiseuille equation has been commonly employed to characterize capillary flow in smooth tubes. For non-smooth tubes, as the equation remains valid when $|dR/dz| << 1$ (Figliuzzi and Buie 2013), the fully-developed fluid velocity along a conical tube with small undulations may be obtained as:

$$w(r) = \frac{1}{4\eta}\left(r^2 - R^2\right)\frac{dp}{dz}, \tag{6}$$

where η is the dynamic viscosity of fluid, and r is the radial position in cylindrical coordinates (Fig. 3).

The stress tension exerted on the undulated wall is given by $\tau = \eta\, dw/dr|_{r=R(z)}$, which includes an unknown factor dp/dz (cf. Equation (6)). To express dp/dz as a function of capillary height h, the concept that the volumetric flow rate is equal at every cross-section of the undulated conical tube is applied, yielding:

$$Q = \pi R^2(h)\dot{h} = -\frac{\pi R^4(z)}{8\eta}\frac{dp}{dz}. \tag{7}$$

Thus, the viscous force exerted on the fluid can be obtained, as:

$$F_{vis} = 8\pi\eta R^2(h)\dot{h}\int_0^h \frac{1}{R^2(z)}dz. \tag{8}$$

The gravity of the fluid in the control volume is:

$$F_g = \pi\rho G\sin(\phi)\int_0^h R^2(z)dz. \tag{9}$$

Substituting Eqs. (3), (5), (8), and (9) into Eq. (1), and taking the capillary force as a scaler, leads to:

$$\frac{a}{f_0}\frac{d\left(\int_0^h\left[1+\beta\frac{z}{R_0}-\varepsilon\cos\left(\alpha\frac{z}{R_0}\right)\right]^2 dz\dot{h}\right)}{dt} + b\frac{f_1}{f_0}h\dot{h} + c\frac{f_2}{f_0}h\sin(\phi) = 1, \tag{10}$$

where

$$a = \frac{\rho R_0}{2\gamma\cos(\theta)}, b = \frac{4\eta}{R_0\gamma\cos(\theta)}, c = \frac{\rho G R_0}{2\gamma\cos(\theta)},$$

and

$$f_0(h) = \frac{\cos(\varphi)}{\cos(\theta)}\left[1+\beta\frac{h}{R_0} - \varepsilon\cos\left(\alpha\frac{h}{R_0}\right)\right],$$

$$f_1(h) = \frac{R^2(h)}{h}\int_0^h \frac{1}{R^2(z)}dz,$$

$$f_2(h) = \frac{1}{R_0^2 h}\int_0^h R^2(z)dz.$$

In the limit when ε and β are both equal to 0, the problem becomes capillary flow in a smooth tube, with f_1, f_2, and f_3 all equaling to unity. Equation (10) then simplifies to:

$$a\frac{d\left(h\dot{h}\right)}{dt} + bh\dot{h} + ch\sin(\phi) = 1, \tag{11}$$

which is consistent with existing results (e.g., Fries and Dreyer 2009). When $t \to \infty$, the rising fluid reaches a steady height, whereby both the inertial and viscous forces vanish. For a vertical conical tube, the steady height is obtained by solving $h_{eq} = 2\gamma\cos(\theta)/\left(\rho G R_0\right)$.

Dimensionless models of capillary rise in both smooth and roughened tubes can be developed by introducing a dimensionless number to quantify the influence of inertial force, defined as (Fries and Dreyer 2009):

$$\Omega = \sqrt{\frac{b^2}{ac^2}} = \sqrt{\frac{128\gamma\cos(\theta)\eta^2}{\rho^3 G^2 R_0^5}}.$$

Built upon this nondimensionalization approach, the effects of opening angle, amplitude and wave number of undulations on capillary flow are quantified using the theoretical model developed above. To this end, the viscous and gravitational forces are selected as scaling parameters, so that the dimensionless rising height h^* and the corresponding dimensionless time t^* can be expressed as:

$$h^* = ch = \frac{\rho G R_0}{2\gamma\cos(\theta)}h = \frac{h}{h_0}, \tag{12}$$

$$t^* = \frac{c^2}{b}t = \frac{\rho^2 G^2 R_0^3}{16\eta\gamma\cos(\theta)}t = \frac{t}{t_0}. \tag{13}$$

The apparent contact angle φ expressed in terms of h^* and t^* is thence:

$$\varphi = \theta + \arctan\left[\frac{\frac{2\beta}{\mathrm{Bo}}\cos(\theta)}{+\varepsilon\frac{2\alpha}{\mathrm{Bo}}\cos(\theta)\sin\left(\frac{2\alpha}{\mathrm{Bo}}\cos(\theta)h^*\right)}\right], \tag{14}$$

where $\mathrm{Bo} = \rho G R_0^2/\gamma$ is the Bond number measuring the relationship between gravity and surface tension, i.e., a small Bo ($<<1$) indicates capillary force is dominant, while a large Bo means gravity is dominant. It follows that Eq. (10) can be rewritten in dimensionless form, as:

$$\frac{\frac{1}{\Omega^2 f_0(h^*)}\frac{d\left(\int_0^{h^*} R^{*2}(z^*)dz^*\dot{h}^*\right)}{dt^*}}{+\frac{f_1(h^*)}{f_0(h^*)}h^*\dot{h}^* + \frac{f_2(h^*)}{f_0(h^*)}h^*\sin(\phi) = 1}, \tag{15}$$

where

$$f_0(h^*) = \frac{\cos(\varphi)}{\cos(\theta)}\left[\begin{array}{c} 1+\frac{2\beta}{\mathrm{Bo}}\cos(\theta)h^* \\ -\varepsilon\cos\left(\frac{2\alpha}{\mathrm{Bo}}\cos(\theta)h^*\right)\end{array}\right], \tag{16}$$

$$f_1(h^*) = \frac{R^{*2}(h^*)}{h^*}\int_0^{h^*}\frac{1}{R^{*2}(z^*)}dz^*, \tag{17}$$

$$f_2(h^*) = \frac{1}{h^*}\int_0^{h^*} R^{*2}(z^*)dz^*. \tag{18}$$

As shown in Eq. (15), Ω appears in the inertial term to measure the effect of inertia. In other words, inertial effect is important if Ω is small (e.g., Ω = 0.1) and insignificant if Ω is large (e.g., Ω = 100).

Numerical Results and Discussion

A. Details of numerical simulation

To validate the theoretical model developed in the previous section, numerical simulations of dynamic capillary flow in roughened conical tubes are performed with the commercially available COMSOL Multiphysics. Due to axial symmetry, the problem is taken as two-dimensional (2D), and the corresponding physical model is displayed in Fig. 4. The "Laminar flow" of the module "Two-Phase Flow, Phase Field" in COMSOL is utilized, including "Laminar Flow" and "Phase Field". The liquid is water at room temperature ($\rho_l = 1000$ kg·m^{-3}, $\eta_l = 0.001$ Pa·s, $\gamma = 72$ mN·m^{-1}), and the gas is air (obtained in the Built-in material). Boundary conditions adopted in "Laminar Flow" and "Phase Field" models are presented in Table 1. Depending surface treatment and surface properties, the static contact angle θ between a given liquid and a given substrate material of channel wall typically exhibits a value varying within a range, e.g., $0° < \theta < 90°$ for hydrophilic surfaces and $90° < \theta < 180°$ for hydrophobic surfaces. In the current study, for the water–glass combination considered, the static contact angle is assumed to have a fixed value of 67.5° (Martinez 2009). The simulation domain is meshed via a hybrid grid, with the fluid container modelled using a mapped mesh and the undulated component using a free triangular mesh (Fig. 4).

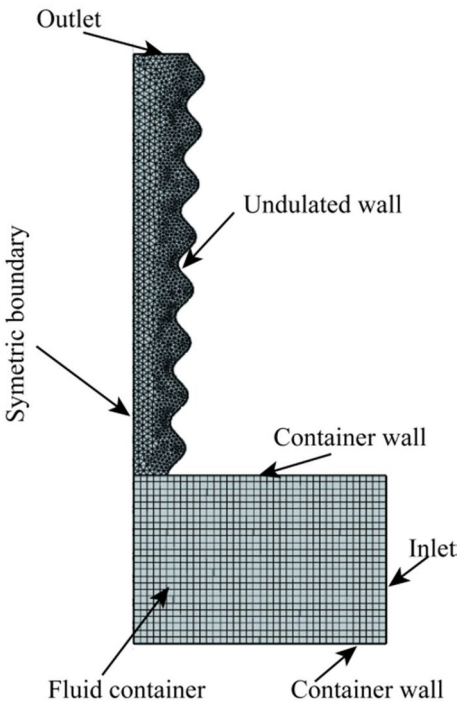

Fig. 4 Schematic of numerical model for a circular conical tube with undulations on its inner wall meshed by a hybrid grid. The mean radius R_0 is 0.5 mm, the cone opening angle β is 0.05, the dimensionless amplitude ε is 0.2, and the dimensionless wave number α is 5

B. Theoretical model versus numerical simulation

For a smooth circular tube under normal gravity ($G = 1$ g), Fig. 5 compares the capillary heights, plotted as functions of time, that are separately obtained using numerical simulations, the LW model, and the present theoretical model, i.e., Eq. (11). The mean radius R_0 of the tube is selected as 500 μm and 250 μm, respectively. As shown in Fig. 5a, when the mean tube radius is relatively large ($R_0 = 500$ μm), the capillary rising height increases with time, and exhibits oscillation during the initial stage ($t < 0.2$ s) except for that predicted with the LW model. When the radius is reduced to 250 μm, as shown in Fig. 5b, such oscillation does not

Table 1 Boundary conditions for numerical model (ρ_l is density of liquid, and Φ is phase field variable: liquid, 1; gas, -1)

Boundaries	Laminar Flow	Phase Field
Undulated wall	No slip	Wetted wall
Container wall	No slip	Wetted wall
Inlet	$p = GZ\rho_l$	$\Phi = 1$
Outlet	$p = 0$	$\Phi = -1$
Symmetry type	Axial symmetry	Axial symmetry

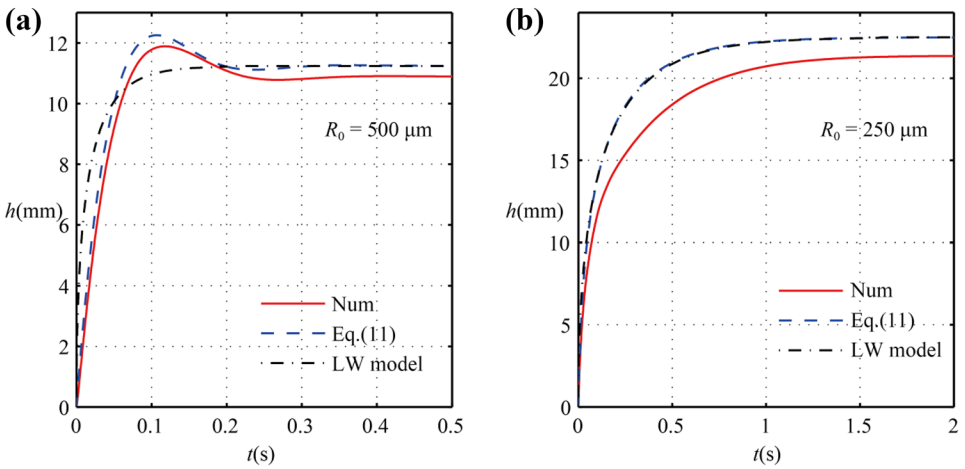

Fig. 5 Comparison of capillary rises obtained by numerical simulations, the LW model, and Eq. (11) in a smooth tube with radius: **a** 500 μm and **b** 250 μm. The static contact angle is assumed to be 67.5°

occur, which is consistent with the LW model that neglects inertial effect. That is, inertial effect becomes less significant as tube radius is reduced. For both tube radii considered, the numerically calculated capillary height is consistently smaller than that predicted using either the LW model or Eq. (11), including the steady height. This is attributed to the fact that both the LW model and Eq. (11) are established based on the assumption that the flow is fully developed and the effect of entry and exit losses is negligible. It is also found that, in the case of large radius (500 μm), the discrepancy between theoretical and numerical results is less than that of small radius (250 μm). The reason is that, the length-to-diameter ratio in the case of large radius is smaller and the exit/entry losses are less, thus enabling a smaller discrepancy (Han and Charles 1971). Nonetheless, overall, the numerical simulations confirm that Eq. (11) is viable for exploring the dynamics of capillary flow in smooth tubes. Next, for conical tubes having undulated inner walls, the numerical simulation results are compared with theoretical predictions (i.e., Eq. (15)).

III. Effect of undulation on capillary flow in conical tubes

1. Comparison of steady capillary height between theoretical and numerical results

With particular focus placed upon the effect of hypergravity on dynamic capillary rising, the case of $G = 10\ g$ gravity is taken as an example to check the validity of analytical model predictions against numerical simulation results. According to Eqs. (14)−(18), the dimensionless capillary rise h^* is dependent upon the non-dimensional numbers Bo and Ω. The basic physical properties of several commonly used liquids at room temperature are summarized in Table 2, which are then used to calculate the values of Bo and Ω for selected channel sizes (Table 3).

For relatively small values of ε (≤ 0.1), α (≤ 1) and β (positive, ≤ 0.05), Table 4 compares the theoretically predicted dimensionless steady heights with numerical simulation results. When α is sufficiently small (e.g., $\alpha = 0.1$), the steady height in an undulated conical tube is larger than that in its smooth counterpart, increasing with increasing ε for all β values considered. For such small values of α, the wavelength of undulation is relatively large; correspondingly, the local radius on the undulated surface of a conical tube is smaller than $R_0 + \beta h$, which remains almost unchanged during the whole process of capillary rising. In addition, a larger ε means a smaller local radius and hence a larger capillary force and higher steady height. In contrast, the results presented in Table 4 suggest that, when α is relatively large (e.g., ≥ 0.5), the steady height decreases with increasing ε and/or β. In other words, the static flow resistance is enlarged when the undulation becomes denser and/or the amplitude of undulation is increased. Moreover, when the opening angle is increased, the local radius is enlarged and hence the capillary force drops, resulting in a lower steady height.

The results of Table 4 also show that the discrepancy between theoretical and numerical steady heights decreases with increasing β. A larger β means a larger local radius

Table 2 Physical properties of commonly used liquids at room temperature (298.15 K)

	ρ (kg·m^{-3})	η (mPa·s)	γ (mN·m^{-1})
Water	1000	0.1	72
Lubricant oil	885	130	25.6
Castor oil	957	750 ± 0.05	33.8
Decane	729	0.888	23.8
Toluene	865	0.5503	28.7
Diethyl ether	722	0.267	18.0
Dioxane	1033	1.18	32.5

Table 3 Values of dimensionless numbers Ω and Bo for commonly used liquids ($G = 10\ g$). Here θ is the static contact angle

	θ (°)	Ω			Bo		
		50 μm	500 μm	5 mm	50 μm	500 μm	5 mm
Water	0	55.41	0.18	0.0006	0.003	0.34	34.03
	67.5	34.28	0.11	0.0003	0.003	0.34	34.03
Lubricant oil	0	5159.43	16.32	0.052	0.009	0.85	84.69
	60	3648.27	11.64	0.036	0.009	0.85	84.69
Castor oil	0	30,416	96.18	0.302	0.007	0.69	69.37
	60	21,507	68.01	0.221	0.007	0.69	69.37
Decane	0	45.45	0.14	0.0005	0.008	0.75	75.04
	60	32.14	0.10	0.0003	0.008	0.75	75.04
Toluene	0	23.93	0.08	0.0002	0.007	0.74	73.84
	60	16.92	0.05	0.0002	0.007	0.74	73.84
Diethyl ether	0	12.06	0.04	0.0001	0.01	0.98	98.27
	60	8.53	0.03	0.00009	0.01	0.98	98.27
Dioxane	0	41.84	0.13	0.0004	0.008	0.78	77.87
	60	29.59	0.09	0.0003	0.008	0.78	77.87

and hence smaller length-to-diameter ratio, which causes a smaller pressure drop across the tube (Han and Charles 1971). Accordingly, the discrepancy between theory and simulation is reduced. In contrast, the discrepancy decreases with increasing ε and α. Therefore, how to make the discrepancy disappear becomes a complex issue, as discussed previously by Ramakrishnan et al. (2019) for smooth tubes. For simplicity, in the current study, we only discuss how key

Table 4 Comparison between theoretical and numerical results of dimensionless steady height for different geometric parameters of undulated conical tube ($G = 10\ g$). Equation (15), Num, and Gap represent the present theoretical results obtained by Eq. (15), numerical simulations, and the discrepancy between them, respectively. Here, Gap = (Eq. (15)—Num) / Eq. (15) × 100

	$\alpha = 0.1$								
	$\beta = 0.01$			$\beta = 0.025$			$\beta = 0.05$		
ε	Equation (15)	Num	Gap(%)	Th	Num	Gap(%)	Equation (15)	Num	Gap(%)
0	0.9453	0.8828	6.61	0.8621	0.8192	4.98	0.7222	0.6950	3.77
0.01	0.9537	0.8904	6.64	0.8698	0.8264	4.99	0.7286	0.7024	3.60
0.025	0.9666	0.9004	6.85	0.8815	0.8382	4.92	0.7383	0.7100	3.87
0.05	0.9890	0.9231	6.66	0.9018	0.8575	4.92	0.7551	0.7285	3.52
0.075	1.0125	0.9467	6.50	0.9230	0.8790	4.78	0.7727	0.7479	3.21
0.1	1.0371	0.9704	6.43	0.9453	0.9005	4.74	0.7911	0.7661	3.16
	$\alpha = 0.5$								
	$\beta = 0.01$			$\beta = 0.025$			$\beta = 0.05$		
ε	Equation (15)	Num	Gap(%)	Equation (15)	Num	Gap(%)	Equation (15)	Num	Gap(%)
0.01	0.9321	0.8736	6.27	0.8490	0.8150	4.01	0.7099	0.6942	2.21
0.025	0.9124	0.8660	5.09	0.8294	0.8079	2.59	0.6919	0.6906	0.19
0.05	0.8795	0.8527	3.05	0.7975	0.7973	0.03	0.6631	0.6897	-4.01
0.075	0.8471	0.8412	0.70	0.7666	0.7868	-2.63	0.6359	0.6767	-6.41
0.1	0.8156	0.8299	-1.75	0.7370	0.7782	-5.59	0.6103	0.6693	-9.67
	$\alpha = 1$								
	$\beta = 0.01$			$\beta = 0.025$			$\beta = 0.05$		
ε	Equation (15)	Num	Gap(%)	Equation (15)	Num	Gap(%)	Equation (15)	Num	Gap(%)
0.01	0.9081	0.8560	5.73	0.8191	0.7963	2.79	0.6749	0.6757	-0.12
0.025	0.8413	0.8196	2.58	0.7473	0.7628	-4.49	0.6042	0.6466	-7.02
0.05	0.7121	0.7597	-6.68	0.6251	0.7077	-13.2	0.5003	0.6067	-21.26
0.075	0.5930	0.7028	-18.5	0.5524	0.6554	-18.7	0.4204	0.5559	-32.24
0.1	0.5011	0.6511	-29.9	0.4446	0.6087	-36.9	0.3607	0.5176	-43.50

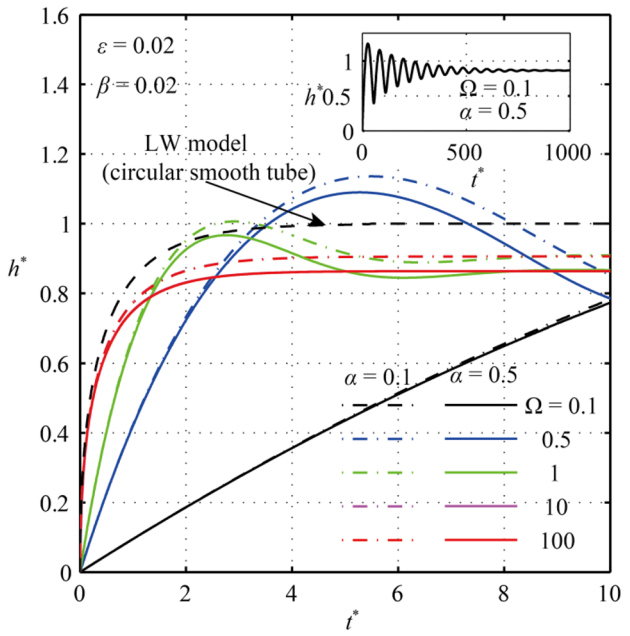

Fig. 6 Dynamic rising in a vertical undulated conical tube for selected values of opening angle β, amplitude ε, and wave number α under different inertial cases. The case of $\Omega=0.1$ and $\alpha=0.5$ is shown over a longer period of time to highlight the steady state

morphological parameters such as ε, α, and β influence the discrepancy between theoretical and numerical results, and do not try to make it vanish.

2. Inertial effect on dynamic capillary rise

How inertial force affects dynamic capillary rise in an undulated conical tube is analyzed next. As the present theoretical model is valid for small values of ε (≤ 0.1), α (≤ 1), and β (≤ 0.05), the rising curve is calculated by applying Eq. (15). For a vertical undulated conical tube, Fig. 6 plots the dimensionless rising height h^* as a function of dimensionless time t^* for selected geometric parameters ($\beta=0.02$, $\varepsilon=0.02$, $\alpha=0.1$ and 0.5) and selected values of dimensionless (inertial) parameter Ω (=0.1, 0.5, 1, 10, 100). For relatively small Ω (e.g., <2), the capillary height first increases, then starts to oscillate, and finally tends to its steady height, but taking a relatively long time to achieve it. In other words, a small Ω indicates a large inertial force, thus causing initial oscillation in capillary rise. With liquid type, temperature, and gravity environment all fixed, a larger mean radius R_0 implies a smaller Ω and, conversely, a smaller R_0 means a larger Ω. Consequently, oscillating capillary rise occurs in an undulated conical tube of large mean radius, but disappears if its mean radius becomes sufficiently small. In addition, the steady height of capillary rise in a conical smooth tube with positive β is always smaller than that (predicted by the LW model) in a circular smooth tube, because the radius of the former gradually expands, leading to a smaller capillary force.

3. Effect of enlarged morphological parameters

Although the effect of hypergravity on capillary rising and steady height have hitherto been theoretically predicted for relatively small values of ε, α, and β, how the predictions are affected when the values of these parameters are increased remains elusive. Therefore, it is necessary to increase the values of ε, α, and β beyond the ranges considered by the present theoretical model (e.g., $\varepsilon\sim0.3$ and $\alpha\sim10$), and then perform direct numerical simulations. Table 5 presents the numerically calculated steady height

Table 5 Numerical simulation results of dimensionless steady capillary height for large geometrical parameters of undulated conical tube

	$\alpha=0.1$			$\alpha=0.5$			$\alpha=1$		
ε	$\beta=0.01$	$\beta=0.025$	$\beta=0.05$	$\beta=0.01$	$\beta=0.025$	$\beta=0.05$	$\beta=0.01$	$\beta=0.025$	$\beta=0.05$
0.15	1.0132	0.9384	0.8315	0.8043	0.7579	0.6802	0.5646	0.5281	0.4818
0.2	1.0696	0.9882	0.8744	0.7928	0.7453	0.6694	0.4976	0.4703	0.4327
0.25	1.1317	1.0419	0.9182	0.7688	0.7243	0.6605	0.4448	0.4216	0.3867
0.3	1.1967	1.0972	0.9662	0.7548	0.7123	0.6471	0.4031	0.3845	0.3533
	$\alpha=5$			$\alpha=8$			$\alpha=10$		
ε	$\beta=0.01$	$\beta=0.025$	$\beta=0.05$	$\beta=0.01$	$\beta=0.025$	$\beta=0.05$	$\beta=0.01$	$\beta=0.025$	$\beta=0.05$
0.01	0.8719	0.7881	0.7124	0.8531	0.7688	0.6851	0.8251	0.7394	0.6460
0.025	0.9102	0.8161	0.7322	0.8991	0.7977	0.7109	0.8366	0.7701	0.6678
0.05	0.9608	0.9138	0.8378	0.9301	0.8673	0.8093	0.9068	0.8181	0.7468
0.1	1.0029	0.9226	0.8557	0.9559	0.9039	0.8210	0.9306	0.8875	0.7639
0.15	1.0039	0.9681	0.9079	0.9702	0.9292	0.8747	0.9546	0.9141	0.8299
0.2	1.0158	0.9935	0.9351	0.9769	0.9359	0.9011	0.9662	0.9179	0.8806
0.25	1.0328	1.0132	0.9773	0.9955	0.9606	0.9321	0.9859	0.9483	0.9095
0.3	1.0406	1.0232	0.9942	1.0262	1.0045	0.9526	1.0020	0.9820	0.9364

Table 6 Theoretically predicted steady heights for negative opening angle β at small ε and α ($G=10\ g$)

	$\alpha=0.1$			$\alpha=0.25$			$\alpha=0.5$		
ε	$\beta=-0.01$	$\beta=-0.025$	$\beta=-0.05$	$\beta=-0.01$	$\beta=-0.025$	$\beta=-0.05$	$\beta=-0.01$	$\beta=-0.025$	$\beta=-0.05$
0.01	1.0633	1.1425	1.265	1.0575	1.1367	1.2594	1.0414	1.1211	1.2457
0.025	1.0778	1.1581	1.2819	1.063	1.1431	1.2677	1.0224	1.1035	1.2323
0.05	1.1029	1.185	1.311	1.0723	1.1541	1.2817	0.9899	1.0726	1.2073
0.075	1.1291	1.2132	1.3415	1.0818	1.1653	1.2961	0.9568	1.0402	1.1793
0.1	1.1566	1.2427	1.3732	1.0915	1.1767	1.3109	0.9236	1.0069	1.1487
	$\alpha=0.75$			$\alpha=1$					
ε	$\beta=-0.01$	$\beta=-0.025$	$\beta=-0.05$	$\beta=-0.01$	$\beta=-0.025$	$\beta=-0.05$			
0.01	1.2457	1.1098	1.2397	1.0277	1.2554	1.1163			
0.025	1.2323	1.0715	1.2139	0.976	1.2563	1.0822			
0.05	1.2073	0.9974	1.1571	0.8509	1.2452	0.9805			
0.075	1.1793	0.9147	1.0819	0.7062	1.1537	0.8181			
0.1	1.1487	0.8316	0.9928	0.588	0.8889	0.6682			

of water in a vertically placed undulated conical tube, under hypergravity ($G=10\ g$). When $\alpha=0.1$ (small wave number of undulation), the steady height is seen to increase with increasing ε, but decrease by increasing both ε and α when $0.5\le\alpha<1$. When $\alpha>5$ (large wave number of undulation), the steady height increases with increasing ε, but decreases as both α and β are increased. In other words, when the undulation has a relatively small wave number (e.g., $\alpha<1$), the theoretically predicted variation trend of steady height with ε, α, and β can be expanded from small values to large values. However, when the wave number α becomes sufficiently large, the trend is significantly altered. The larger the wave number, the denser the undulation, so that more local radii $R_0+\beta h-e$ are smaller than $R_0+\beta h$, leading to a larger capillary force. Also note that, when α is enlarged, the static flow resistance is enhanced. All in all, the variation trend of steady height at large α is more complicated than that predicted by the theoretical model.

As expected, the steady height in a conical tube is larger than that in a circular tube when the diameter of the former is gradually reduced, i.e., β is negative (Table 6). Moreover, the steady height increases as the absolute value of β is increased, because the capillary force increases with decreasing local radius, so that the fluid can rise higher to balance the gravity. Note also that, the influence law of undulation amplitude ε and wave number α on steady height obtained previously for the case of positive β remains valid when β becomes negative (i.e., negative opening angle; Fig. 3b).

4. Capillary rising for selected liquids

Built upon theoretical modeling of hypergravity effect on dynamic capillary rise in conical tubes with idealized undulation morphologies, the ultimate goal of the current study is to provide worthwhile theoretical guidance for practical applications. Figure 7 presents therefore the theoretically predicted capillary rising heights for several commonly used liquids, including water, decane, toluene, diethyl ether, dioxane, lubricant oil, and Castor oil, with the hypergravity fixed at $G=10\ g$. To ensure the validity of the model predictions, only vertical conical tubes with small values of ε (≤0.1), α (≤1), and β (≤0.05) are considered for the plotting. It is seen from Fig. 7 that different liquids exhibit not only significantly different steady heights, but also take different time periods to achieve steady state. These results are

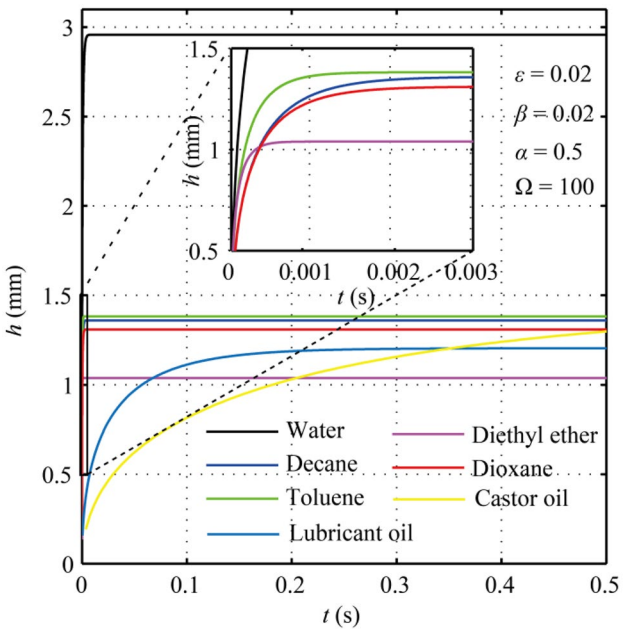

Fig. 7 Dynamic capillary rise in vertical undulated conical tube for several commonly used liquids ($G=10\ g$)

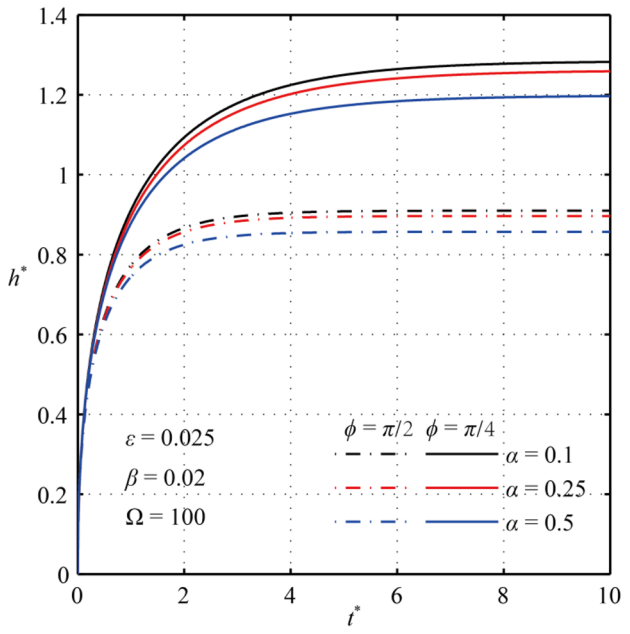

Fig. 8 Dynamic rising in an undulated conical tube (opening angle $\beta = 0.02$ and amplitude $\varepsilon = 0.025$) for selected values of wave number α (=0.1, 0.25, 0.5) and inclination angle ϕ ($\pi/2$ and $\pi/4$), with inertial effect neglected (i.e., $\Omega = 100$)

expected to be of practical significance for hypergravity-sensitive applications in a wide range of fields, especially aeronautical engineering and space exploitation.

For an inclined conical tube, as shown in Fig. 8, the steady capillary height always exceeds that in a vertical tube having identical geometric parameters. Similar conclusion was reached in our previous study (Lei et al. 2021) on dynamic capillary rise in an undulated circular tube, with hypergravity effect neglected.

Finally, although the results of undulated conical tubes presented hitherto are obtained for the selected hypergravity case of $G = 10\ g$, it has been established that the influence law can be conveniently extended to cover other gravity conditions, with lower (larger gravity) or higher (smaller gravity) steady height obtained for undulated conical tubes having identical geometric parameters. For brevity, these results are not shown here.

Concluding Remarks

Blood vessels of human brain and leaf veins of plants are typically represented by undulated conical tubes. Under hypergravity, a theoretical model of dynamic capillary flow in inclined conical tubes having idealized undulated inner walls has been established, with inertial, viscous and gravitational forces duly account for. A dimensionless number combining the three forces is introduced to measure the influence of inertial force. The validity of model predictions is checked against results obtained by performing direct numerical simulations, with good agreement achieved. The validated model is then employed to quantify the effects of several key morphological parameters on dynamic capillary rise, including cone opening angle (positive or negative) and amplitude and wave number of wall undulations, when these parameters take relatively small values. To cover larger values of morphological parameters not considered by the theoretical model and account for both entry and exit losses, additional numerical simulations are carried out. Also, in the presence of hypergravity effect, to promote fundamental understanding of plants nutrient uptake in hypergravity and blood flow in human brain, capillary rising heights of several commonly used liquids are calculated using the proposed theoretical model.

Like most relevant studies, the present study adopts a fundamental assumption: the capillary tube is straight and has rigid walls. In reality, human blood vessels are not only wavy (cf. Figure 1) but also soft such that, when capillary flow of blood is initiated, the capillary force may deform the blood vessel which in turn, affects the capillary flow. In other words, blood transport in human capillaries is critically dependent upon fluid–structure interaction. This issue will be addressed in a future study.

Acknowledgements This work was financially supported by the National Natural Science Foundation of China (Grant Nos. 12032010, 11902155, and 51676156), the Research Fund of State Key Laboratory of Mechanics and Control of Mechanical Structures (MCMS-I-0222K01), the Natural Science Foundation of Jiangsu Province (BK20190382), and by the Priority Academic Program Development of Jiangsu Higher Education Institutions (PAPD).

Data Availability The datasets generated during and/or analyzed during the current study are available from the corresponding author on reasonable request.

Declarations

Conflict of Interests The authors declare no conflict of interest.

References

Akparibo, I. Y., Anderson, J. and Chumbley, E.: Aerospace Gravitational Effects. NCBI StatPearls (2021)

Ando, Y., Okada, H., Takemura, G., Suzuki, K., Takada, C., Tomita, H., Zaikokuji, R., Hotta, Y., Miyazaki, N., Yano, H., Muraki, I., Kuroda, A., Fukuda, H., Kawasaki, Y., Okamoto, H., Kawaguchi, T., Watanabe, T., Doi, T., Yoshida, T., Ushikoshi, H., Yoshida, S., Ogura, S.: Brain-specific ultrastructure of capillary endothelial glycocalyx and its possible contribution for blood brain barrier. Sci. Rep. **8**, 17523 (2018)

Bico, J., Thiele, U., Quéré, D.: Wetting of textured surfaces. Colloid. Surf. A **206**, 41–46 (2002)

Bosanquet, C.H.: LV On the flow of liquids into capillary tubes. J. Philos. Mag. **45**, 525–531 (1923)
Bureau, L., Coupier, G., Dubois, F., Duperray, A., Farutin, A., Minetti, C., Misbah, C., Podgorski, T., Tsvirkun, D., Vysokikh, M.: Blood flow and microgravity. C. R. Mecanique **345**, 78–85 (2017)
Cassot, F., Lauwers, F., Fouard, C., Prohaska, S., Lauwers-Cances, V.: A novel three-dimensional computer-assisted method for a quantitative study of microvascular networks of the human cerebral cortex. Microcirculation **13**, 1–18 (2006)
Culbertson, C.T., Tugnawat, Y., Meyer, A.R., Roman, G.T., Ramsey, J.M., Gonda, S.R.: Microchip separations in reduced-gravity and hypergravity environments. Anal. Chem. **77**, 7933–7940 (2005)
Downey, P.J., Levine, L.H., Musgrave, M.E., Mckeon-Bennett, M., Moane, S.: Effect of hypergravity and phytohormones on isoflavonoid accumulation in soybean (Glycine max. L.) callus. Microgravity Sci. Tec. **25**, 9–15 (2013)
Feng, S., Zhu, P., Zheng, H., Zhan, H., Chen, C., Li, J., Wang, L., Yao, X., Liu, Y., Wang, Z.: Three-dimensional capillary ratchet-induced liquid directional steering. Sicience **373**, 1344–1348 (2021)
Figliuzzi, B., Buie, C.R.: Rise in optimized capillary channels. J. Fluid Mech. **731**, 142–161 (2013)
Fries, N., Dreyer, M.: Dimensionless scaling methods for capillary rise. J. Colloid Interf. Sci. **338**, 514–518 (2009)
Guo, X., Deng, C., Fan, Y., Mu, Y., Fan, N.: Experimental research on leaf vein geometric characteristics of multibranch horizontal well for coalbed methane recovery. Energy Sci. Eng. **7**, 2921–2935 (2019)
Han, C.D., Charles, M.: Entrance-and exit-correction in capillary flow of molten polymers. Trans. Soc. Rheol. **15**, 371–384 (1971)
Hartmann, D.A., Berthiaume, A., Grant, R.I., Harrill, S.A., Koski, T., Tieu, T., Mcdowell, K.P., Faino, A.V., Kelly, A.L., Shih, A.Y.: Brain capillary pericytes exert a substantial but slow influence on blood flow. Nat. Neurosci. **24**, 633–645 (2021)
Hay, K.M., Dragila, M.I., Liburdy, J.: Theoretical model for the wetting of a rough surface. J. Colloid Interf. Sci. **325**, 472–477 (2008)
Heshmati, M., Piri, M.: Experimental Investigation of Dynamic Contact Angle and Capillary Rise in Tubes with Circular and Noncircular Cross Sections. Langmuir **30**, 14151–14162 (2014)
Iceri, D.M., Zummo, G., Saraceno, L., Ribatski, G.: Convective boiling heat transfer under microgravity and hypergravity conditions. Int. J. Heat Mass Tran. **153**, 119614 (2020)
Kim, H.K., Park, J., Hwang, I.: Investigating water transport through the xylem network in vascular plants. J. Exp. Bot. **65**, 1895–1904 (2014)
Kim, J., Moon, M., Kim, H.: Capillary rise in superhydrophilic rough channels. Phys. Fluids **32**, 032105 (2020)
Kundan, A., Plawsky, J.L., Wayner, P.C.: Effect of capillary and Marangoni forces on transport phenomena in microgravity. Langmuir **31**, 5377–5386 (2015)
Lei, J., Xu, Z., Xin, F., Lu, T.J.: Dynamics of capillary flow in an undulated tube. Phys. Fluids **33**, 052109 (2021)
Liou, W.W., Peng, Y., Parker, P.E.: Analytical modeling of capillary flow in tubes of nonuniform cross section. J. Colloid Interf. Sci. **333**, 389–399 (2009)
Lucas, R.: Ueber das Zeitgesetz des kapillaren Aufstiegs von Flüssigkeiten. Kolloid-Z. **23**, 15–22 (1918)
Malijevský, A.: Does surface roughness amplify wetting? J. Chem. Phys. **141**, 184703 (2014)
Martinez, N.: Wettability of silicon, silicon dioxide, and organosilicate glass. University of North Texas, Diss (2009)
Oikonomidou, O., van Loon, J.J.W.A., Schwarz, C.J., Kostoglou, M., Karapantsios, T.D.: A note on liquid velocities arising during decompression degassing in hypergravity. Microgravity Sci. Tec. **31**, 505–515 (2019)
Ouali, F.F., Mchale, G., Javed, H., Trabi, C., Shirtcliffe, N.J., Newton, M.I.: Wetting considerations in capillary rise and imbibition in closed square tubes and open rectangular cross-section channels. Microfluid. Nanofluid. **15**, 309–326 (2013)
Patel, T., Patel, D., Thakkar, N., Lakdawala, A.: A numerical study on bubble dynamics in sinusoidal channels. Phys. Fluids **31**, 052103 (2019)
Peyrounette, M., Davit, Y., Quintard, M., Lorthois, S.: Multiscale modelling of blood flow in cerebral microcirculation: Details at capillary scale control accuracy at the level of the cortex. PLoS ONE **13**, e189474 (2018)
Quéré, D.: Inertial capillarity. J. Europhys. Lett. **39**, 533–538 (1997)
Ramakrishnan, T.S., Wu, P., Zhang, H., Wasan, D.T.: Dynamics in closed and open capillaries. J. Fluid Mech. **872**, 5–38 (2019)
Reyssat, M., Courbin, L., Reyssat, E., Stone, H.A.: Imbibition in geometries with axial variations. J. Fluid Mech. **615**, 335–344 (2008)
Shen, A., Liu, Y., Qiu, X., Lu, Y., Liang, S.: A model for capillary rise in nano-channels with inherent surface roughness. Appl. Phys. Lett. **110**, 121601 (2017)
Shuttleworth, R., Bailey, G.L.J.: The spreading of a liquid over a rough solid. Discuss. Faraday Soc. **3**, 16–22 (1948)
Sudeepthi, A., Yeo, L., Sen, A.K.: Cassie-Wenzel wetting transition on nanostructured superhydrophobic surfaces induced by surface acoustic waves. Appl. Phys. Lett. **116**, 93704 (2020)
van Geel, M.H.A., Giannopapa, C.G., van der Linden, B.J., Kroot, J.M.B.: Development of a blood flow model including hypergravity and validation against an analytical model. PVP2010–26149 **4**, 109–115 (2010)
Vidyasagar, P.B., Jagtap, S.S., Dixit, J.P., Kamble, S.M., Dhepe, A.P.: Effects of short-term hypergravity exposure on germination, growth and photosynthesis of Triticum aestivum L. Microgravity Sci. Tec. **26**, 375–384 (2014)
Wang, Q., Graber, E.R., Wallach, R.: Synergistic effects of geometry, inertia, and dynamic contact angle on wetting and dewetting of capillaries of varying cross sections. J. Colloid Interf. Sci. **396**, 270–277 (2013)
Washburn, E.W.: The dynamics of capillary flow. Phy. Rev. **17**, 273–283 (1921)
Wenzel, R.N.: Resistance of solid surface to wetting water. Ind. Eng. Chem. **28**, 988–994 (1936)